Journal of Alloys and Compounds 509 (2011) 123–127

Contents lists available at ScienceDirect

Journal of Alloys and Compounds

journal homepage: www.elsevier.com/locate/jallcom

The phase transformations and cycling performance of copper–tin alloy anode materials synthesized by sputtering

Yu-Sheng Lin[a], Jenq-Gong Duh[a,*], Hwo-Shuenn Sheu[b]

[a] Department of Materials Science and Engineering, National Tsing Hua University, Hsinchu, Taiwan
[b] National Synchrotron Radiation Research Center, Hsinchu Science-Based Industrial Park, Hsinchu, Taiwan

ARTICLE INFO

Article history:
Received 24 July 2010
Received in revised form 25 August 2010
Accepted 28 August 2010
Available online 6 September 2010

Keywords:
Energy storage materials
Thin films
Crystal structure
Synchrotron radiation
Electrochemical reactions
Phase transitions

ABSTRACT

A sputtering technique was adopted to synthesize Sn–Cu thin film electrodes. Island Sn particles were obtained on the copper foil. Cu_6Sn_5 was spontaneously generated at the interface between Sn and Cu foil. To further improve the cycling stability, Cu source was introduced to increase the formation of Cu_6Sn_5 and to serve as a buffer during cycling. Moreover, the phase and elemental ratio of Sn and Cu varied in the synthesized electrode by alternately adjusting sputtering time for Sn and Cu. The cell synthesized by sputtering Sn for 5 min and Cu for 9 s alternately exhibited the best cycling stability. The 1st charge capacity of cell was 635 mA hg^{-1}, and the 1st efficiency was even higher than 97%. The capacity remained higher than 500 mA hg^{-1} after 15 cycles. The phase transformation of cell was investigated through voltage profile, CV curve and in situ XRD analysis. The in situ XRD analysis confirmed that Cu_6Sn_5 could react with lithium directly without the presence of Li_2CuSn during cycling. The reaction mechanism of Cu_6Sn_5 with lithium during cycling was demonstrated to be an alloying process, and the structure of Cu_6Sn_5 was thus a low-temperature monoclinic phase.

1. Introduction

The increasing demand for higher energy density and power density of batteries in electronic devices has attracted investigators to develop new materials for lithium-ion batteries. In commercial lithium-ion batteries, the carbonaceous materials are generally used as anode materials [1]. However, the theoretical capacity of graphite was only 372 mA hg^{-1}. As a result, metallic tin element was used as the anode material, for its higher theoretical capacity, higher lithium packing density and proper operating voltage [2]. Nevertheless, the most critical problems in these materials were the severe volume expansion and contraction during cycling. Because of the large volume change in the Li_XSn alloys, Sn metal particles were pulverized to lose the electric contact with electrode eventually [3,4], which limited the cycle life of the anode. To solve this problem, some researchers were devoted to preparing nanosized Sn particles to reduce the absolute volume change during cycling and further to improve the electrochemical property [5,6]. However, when Sn particles were reduced to nanosizes, the agglomeration of Sn would become serious, causing cracks, pulverization and capacity fading in the Li–Sn alloy electrodes after long cycling [7,8]. It is argued that the method of reducing metallic Sn particle sizes discussed in literature might not be an efficient way to improve cycling performance.

The intermetallic compounds (M′M) could improve cycling stability via absorbing the stress induced by large volume change [9]. The elements M′ and M were inactive and active element, respectively. Cu_6Sn_5 was proven to be one of the promising anode materials due to its high reversibility. In literature, several methods were adopted to synthesize Cu_6Sn_5 as the anode material, including chemical reduction [10,11], electroplating [12,13], electron-beam deposition [14], ball-milling [15] and sputtering [16]. In this study, sputtering was selected to synthesize the Sn–Cu electrode, which was beneficial to form Cu_6Sn_5 spontaneously at the interface between Sn and Cu without any further heat treatment. Besides, adjusting the composition of Sn–Cu alloy could optimize cycling performance by altering its phase using different sputtering time of Sn/Cu.

In addition, the reaction mechanism of Cu_6Sn_5 during cycling could be evaluated by in situ XRD analysis [17,18]. Dahn et al. [18] demonstrated that the reaction of Cu_6Sn_5 with Li during cycling proceeded in two steps. The discharge plateau around 0.4 V was Cu_6Sn_5 transformation into Li_2CuSn. The voltage plateau below 0.1 V was due to Cu extrusion from the Li_2CuSn structure to yield $Li_{4.4}Sn$. According to the binary phase diagram, Cu_6Sn_5 has two structures, i.e., high-temperature hexagonal η-Cu_6Sn_5 and low-temperature monoclinic η′-Cu_6Sn_5. Different structures of Cu_6Sn_5 would normally react with lithium through different paths [15,16].

* Corresponding author at: Department of Materials Science and Engineering, National Tsing Hua University, No. 101, Section 2, Kuang-Fu Road, Hsinchu, Taiwan 30013. Tel.: +886 3 5712686; fax: +886 3 5712686.
E-mail address: jgd@mx.nthu.edu.tw (J.-G. Duh).

0925-8388/$ – see front matter © 2010 Elsevier B.V. All rights reserved.
doi:10.1016/j.jallcom.2010.08.148

Hexagonal η-Cu_6Sn_5 reacted with lithium by forming the intermediate phase of Li_2CuSn, while monoclinic η′-Cu_6Sn_5 reacted with lithium directly without the presence of Li_2CuSn. In this study, in situ XRD analysis was further used to evaluate the phase transformations of Cu_6Sn_5 during cycling and to distinguish the structure of Cu_6Sn_5.

2. Experimental

The copper–tin thin films were prepared by sputtering on copper foil using pure Sn and Cu targets (99.99%, 2 in. in diameter). The gun power of Sn and Cu was 20 W and 100 W, respectively. The working gas was 99.99% pure argon, the gas flow was 20 sccm, and the working pressure was maintained at 6.0×10^{-4} Pa during sputtering. The target-to-substrate distance was fixed at 100 mm. Before loading Cu foil into the chamber, the Cu foil was cleaned by oxalic acid to remove the oxidation layer of copper. As the vacuum was less than 4.8×10^{-6} Pa, bias clean was performed under 500 V for 10 min to remove the oxidation layer again. Moreover, both Sn and Cu targets were pre-sputtered for 2 min to clean the surface of target. Different sputtering time of Sn and Cu was adjusted alternately under constant gun power to change the composition of copper–tin alloy. The total sputtering time was 2 h. Moreover, to reveal the effect of introducing Cu source into Sn-based anode material by sputtering Sn/Cu alternately, the electrode was also deposited only by Sn target for comparison.

The phases were identified with an X-ray diffractometer (XRD, LabX XRD-6000, Shimadzu, Japan) operated at 30 kV and 20 mA using Cu Kα with a wavelength of 1.5406 Å. The deposited amounts of Sn and Cu on the Cu foil were investigated with a newly designed liquid nitrogen free energy dispersive X-ray spectroscopy (X-Max SDD, OXFORD). Morphological observations of Sn–Cu electrodes were observed via scanning electron microscope (SEM, JSM-7600F, JEOL, Japan).

Electrochemical tests were performed using two-electrode of 2016 type coin cells (20 mm in diameter and 1.6 mm in thickness). The cells contained an anode electrode, metallic lithium, polypropylene separator, and electrolyte of 1.0 M $LiPF_6$ in EC/DMC (1:2, vol.%) plus 2 vol.% of VC. The cells were assembled in an argon glove box where both moisture and oxygen content were less than 1 ppm. The cells were cycled between 0.001 V and 1.5 V vs. Li/Li^+ at the rate of 0.1 C during first cycle, and then at the rate of 0.2 C after prolonged cycling. Cyclic voltammetry (CV) measurements were carried out with a potentiostat (Model 263A, EG&G,) at a scanning rate of 0.05 mV s^{-1} in potential range of 0–1.5 V.

The cell designation of in situ XRD experiments was similar to the regular one for the electrochemical test. To have in situ X-ray pass through the cathode electrode, a hole with 4 mm diameter was drilled in the upper cover, bottom cover and Ni spacer of the 2016 coin cell and followed by sealing with a Kapton film. In situ X-ray studies were carried out in the transmission mode at 16 keV (λ = 0.775 Å) in the National Synchrotron Radiation Research Center (NSRRC), Taiwan. The exposure time was 20 s and XRD spectra were recorded on the Mar 345 image plate detector. All in situ X-ray diffraction patterns were calibrated using standard sample (Ag + Si) before further analysis.

3. Results and discussion

3.1. The BEI image and cycling performance of electrode deposited by Sn

Fig. 1 reveals the BEI image of as-deposited electrode which was only deposited by Sn target. From the BEI image, the thickness of the deposited Sn was around 1 μm, and the shape was island structure through BEI image in the observation of cross-section area.

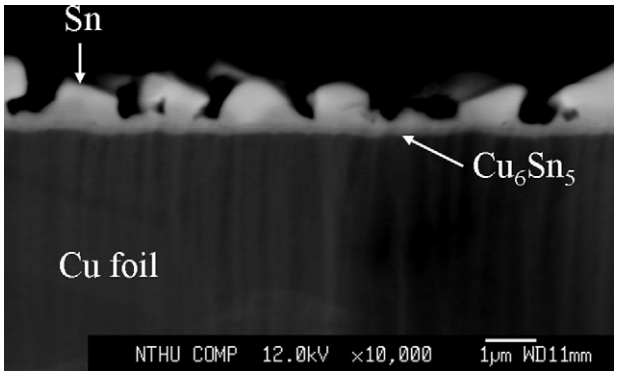

Fig. 1. BEI image of cross-section of electrode which was only deposited by Sn target on the Cu foil.

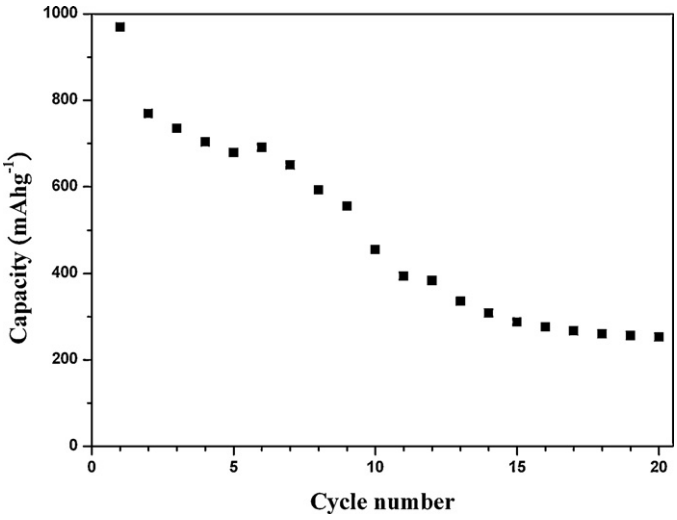

Fig. 2. Cycling performance of cell which was only deposited by Sn target on the Cu foil.

Since the temperature of electrode was very high during sputtering process, the Sn atoms had enough energy to diffuse into the copper matrix and further formed Cu_6Sn_5 at the interface between Sn and Cu. Therefore, the Cu_6Sn_5 with 300 nm in thickness could be revealed at the interface between Sn and Cu foil.

The cycling performance of cell, which was only deposited by Sn target, is displayed in Fig. 2. The 1st capacity was around 970 mA hg^{-1}, which was close to the theoretical capacity of tin (991 mA hg^{-1}). The 10th capacity decreased to 450 mA hg^{-1}. Above half capacity of cell was dropped after 10 cycles, due to the large volume change of Sn during cycling. When the cell was disassembled in an argon glove box, parts of Sn were peeled off and separated from the electrode. In fact, the cycling performance was not good, possibly owing to the small ratio of Cu_6Sn_5/Sn. In other words, insufficient Cu was not able to buffer the volume change during cycling. Therefore, it was thought to introduce the Cu atom into the system to increase the formation of Cu_6Sn_5 and to absorb the large volume change during cycling, which might improve the cycling stability.

3.2. The X-ray diffraction patterns, microstructure observations, and quantitative analysis of samples derived from different sputtering time of Sn/Cu alternately

Fig. 3 presents the X-ray diffraction patterns of samples derived from different sputtering time of Sn/Cu alternately. The phase of Cu_6Sn_5 and Sn was identified through JCPDS card 45-1488 and 04-0673, respectively. In order to distinguish the condition of sample clearly, the sample 3m9s was designated as that the sputtering time of Sn and Cu was 3 min and 9 s, respectively. The major phase of sample 3m9s was Cu_6Sn_5. From the BEI image mentioned above, Cu_6Sn_5 was formed at the interface between Sn and Cu during sputtering process. Therefore, introducing Cu source into the system could further increase the formation of Cu_6Sn_5. However, the counts of Cu_6Sn_5 decreased and that of Sn increased with sputtering time of Sn. As the sputtering time of Sn was above 5 min, the phase of pure metallic Sn became dominant.

SEM images of samples derived from different sputtering time of Sn/Cu alternately is presented in Fig. 4. The morphology of electrode 3m9s displays island structure on the surface of Cu foil, as shown in Fig. 4a, in which the particle size was around 1 μm. As the sputtering time of Sn was increased, the interconnection of particles was also increased. As a result, the particle size of electrode 6m9s was the largest among all conditions, as shown in Fig. 4d.

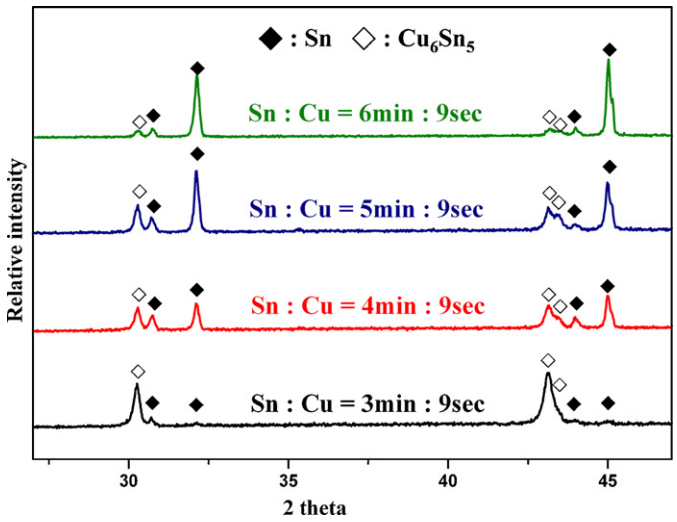

Fig. 3. XRD patterns of sample derived from different sputtering time of Sn and Cu alternately.

EDS analysis was carried out to evaluate the composition of the electrodes derived from different sputtering time of Sn/Cu, and the results are listed in Table 1. The atomic percentage of Sn and Cu of electrode 3m9s was 50.9(7) at.% and 49.0(3) at.%, respectively, which was not equivalent to the atomic ratio of Cu/Sn in Cu_6Sn_5. Most Cu were transformed into Cu_6Sn_5 owing to the elevated temperature during sputtering. Consequently, the electrode 3m9s was composed of Cu_6Sn_5 and pure Sn, as shown in Fig. 3. The results of quantitative analysis indicated that the amount of Sn increased, while Cu decreased with the sputtering time of Sn. The composition of Sn and Cu in the electrode 4m9s were 74.3(7) at.% and 25.6(3) at.%, respectively. As the sputtering time of Sn was 5 min, Sn content increased to 84.0(7) at.% and further raised to 94.2(0) at.% with a sputtering time of 6 min. It was demonstrated that the Sn/Cu ratio of electrode could be controlled by adjusting different sputtering time of Sn and Cu.

Table 1
Quantitative analysis by EDS for samples derived from different sputtering time of Sn and Cu.

Sample designation	Measured composition (at.%)	
3m9s	Sn: 50.9(7)	Cu: 49.0(3)
4m9s	Sn: 74.3(7)	Cu: 25.6(3)
5m9s	Sn: 84.0(7)	Cu: 15.9(3)
6m9s	Sn: 94.2(0)	Cu: 5.8(0)

3.3. The cycling performance of samples derived from different sputtering time of Sn/Cu alternately

The cycling performance of samples derived from different sputtering time of Sn/Cu alternately is displayed in Fig. 5. As compared with the cell only deposited by Sn target, the cycling performance of samples derived from different sputtering time of Sn/Cu alternately was much better. It was demonstrated that the introducing Cu source into Sn-based anode material by sputtering Sn/Cu alternately improved the cycling stability. The cell 5m9s delivered the best cycling performance among all the samples. The 1st charge capacity of cell was around 635 mA hg^{-1}, and 1st efficiency was above 97%. The capacity remained higher than 500 mA hg^{-1} after 15 cycles. The results were attributed to the morphology of elec-

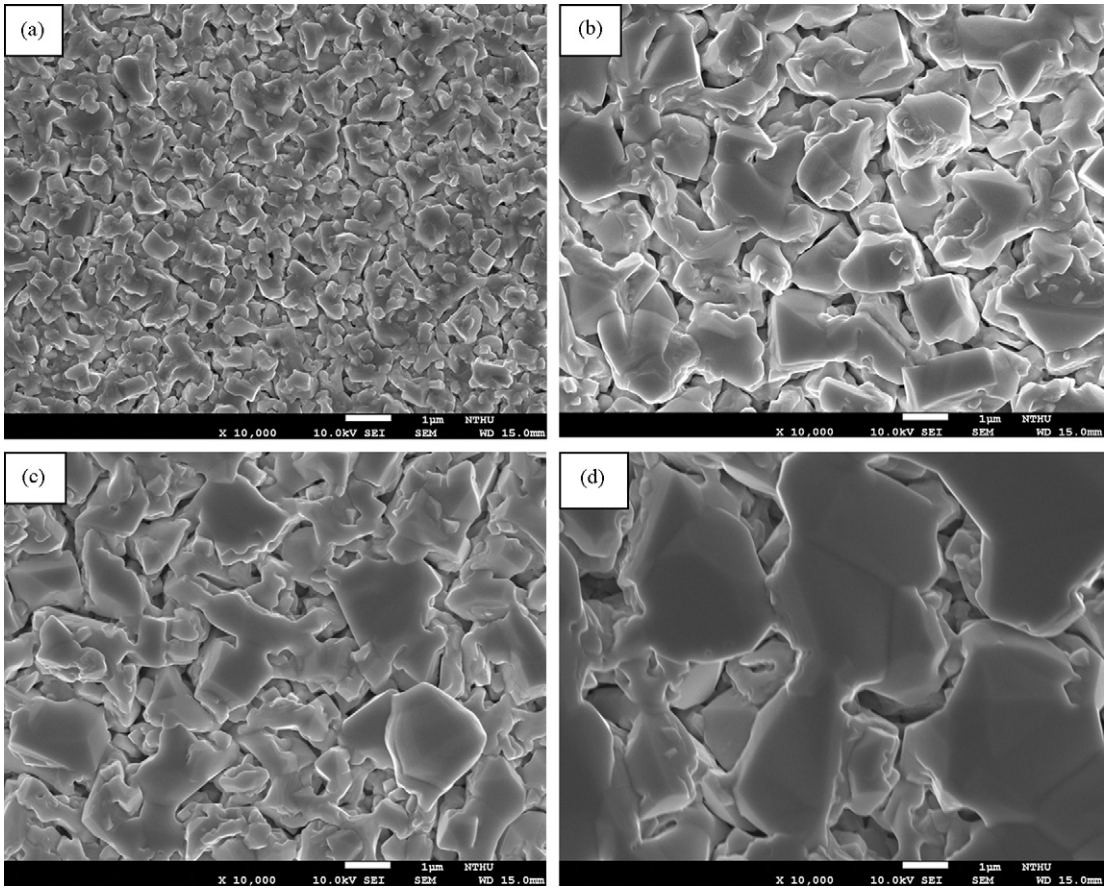

Fig. 4. SEM images of sample derived from different sputtering time of Sn and Cu alternately: (a) 3m9s; (b) 4m9s; (c) 5m9s; (d) 6m9s.

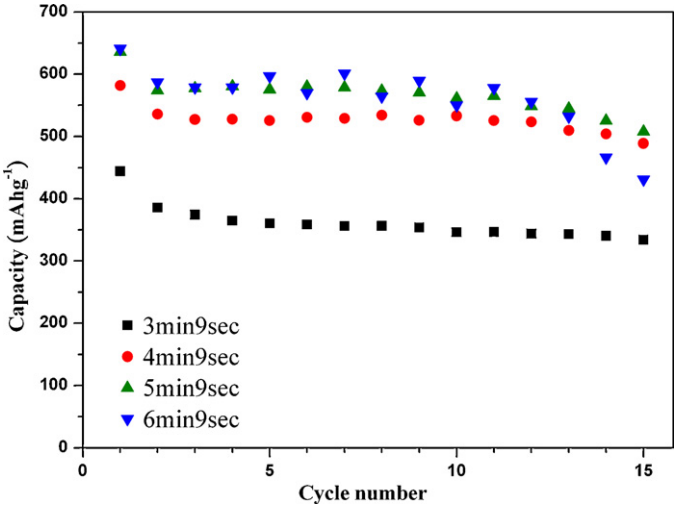

Fig. 5. Cycling performance of sample derived from different sputtering time of Sn and Cu alternately.

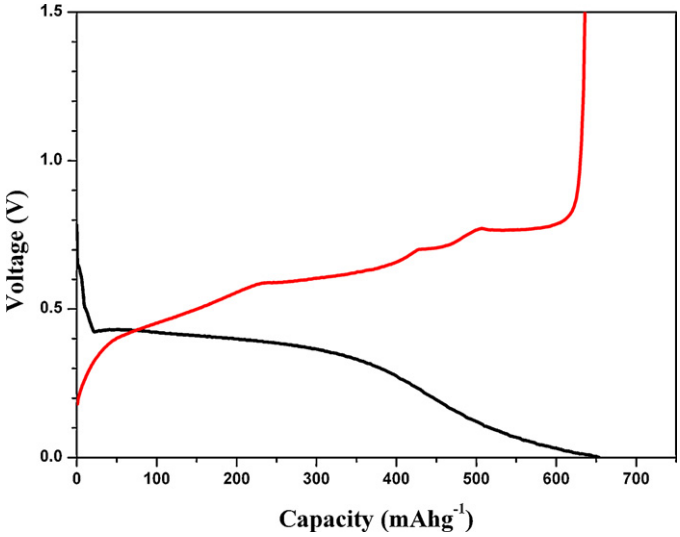

Fig. 6. Initial charge–discharge curve of the Sn–Cu thin film electrode 5m9s cycled between 0 V and 1.5 V vs. Li/Li^+.

trode and the elemental amount adjusted by sputtering time. The island structure provided more space to tolerate the volume change than the layered structure. Besides, introducing Cu into the electrode also enhance the retention. Moreover, existing pure metallic Sn also increased the capacity, and the cycling performance was the best. However, as the sputtering time of Sn increased to 6 min, the cycling performance was poorer than that of 5m9s. Although the initial capacity could be increased by the largest amount of Sn, the smaller ratio of Cu_6Sn_5/Sn led to insufficient buffer for the volume change during cycling. Thus, the capacity fading was revealed after prolonged cycling. The capacity of cell 4m9s was smaller than that of 5m9s, due to less Sn in the electrode. Finally, as the sputtering time of Sn was down to 3 min, the capacity was the smallest among all. The result could be related to the least amount of Sn in the electrode, as shown in Table 1.

3.4. The phase transformation identification of electrode through voltage profile, CV, and in situ XRD

In order to evaluate the phase transformations during cycling of sample 5m9s, the initial charge/discharge curve of the as-deposited Sn–Cu thin film electrode in potential window of 0–1.5 V is shown in Fig. 6. It was apparent that the electrode exhibited three plateaus in the discharge process, i.e., 0.65 V, 0.50 V and 0.35 V. These potential plateaus were close to the formation of Li–Sn phases at room temperature [2]. There were also three potential plateaus at 0.56 V, 0.70 V and 0.77 V, respectively, in the charge process, which might correspond to the delithiation potentials of Li–Sn phases [2]. In fact, the plateaus in the voltage profile were similar to those in pure Sn which was reacted with lithium.

In order to make the phase transformations of electrode 5m9s clearer to be distinguished, CV curve of cell was also performed. Fig. 7 shows the cyclic voltammograms at the rate of 0.5 mV s^{-1} of cell 5m9s. From the CV curve, three reduction peaks at 0.65 V, 0.50 V and 0.35 V could be observed in the cathodic scan, which was related to the generation of Li–Sn materials [14]. Besides, four oxidation peaks in the anodic scan could be displayed at 0.50 V, 0.63 V, 0.73 V and 0.80 V, respectively. These were associated with de-alloying in the Li–Sn materials. From the voltage profile and CV curve mentioned above, it appeared that characteristic reactions during cycling were attributed to Sn. Nevertheless, the phase of electrode 5m9s contained Cu_6Sn_5 and pure metallic Sn, as shown in Fig. 3. Both Cu_6Sn_5 and Sn could react with lithium [2,10–15]. Therefore, the role and the contribution of Cu_6Sn_5 during cycling need to be recognized.

In the binary Sn–Cu phase diagram, Cu_6Sn_5 has two types of structure, i.e., high-temperature hexagonal η-Cu_6Sn_5 and low-temperature monoclinic η′-Cu_6Sn_5. Different structures of Cu_6Sn_5 reacted with lithium through distinct paths during cycling [15,16]. Consequently, the reaction mechanism of Cu_6Sn_5 alloy during cycling could be evaluated in details by in situ XRD pattern, as shown in Fig. 8. The structural changes of copper–tin alloy recognized by the in situ synchrotron X-ray diffraction technique during discharge process at 15th cycle is indicated in Fig. 8a. The in situ XRD patterns revealed sequential phase transformations of copper–tin alloy. The phases were pure Sn and Cu_6Sn_5 at the OCV state. The intensity of Cu_6Sn_5 decreased with lithium insertion. It was demonstrated that Cu_6Sn_5 could participate in the reaction with lithium during cycling. However, the reactions between Cu_6Sn_5 and Li were not displayed in the voltage profile and CV curve. It might be caused by the overlapping of reaction positions of Cu_6Sn_5 and Sn. When the cell was discharged to 0.62 V, Sn and Cu_6Sn_5 were transformed into Li_2Sn_5. As the lithium was further inserted into Li_2Sn_5, the phase of Li_2Sn_5 changed to LiSn at 0.42 V. As the voltage was below 0.37 V, $Li_{4.4}Sn$ alloy showed up with the disappearance of LiSn

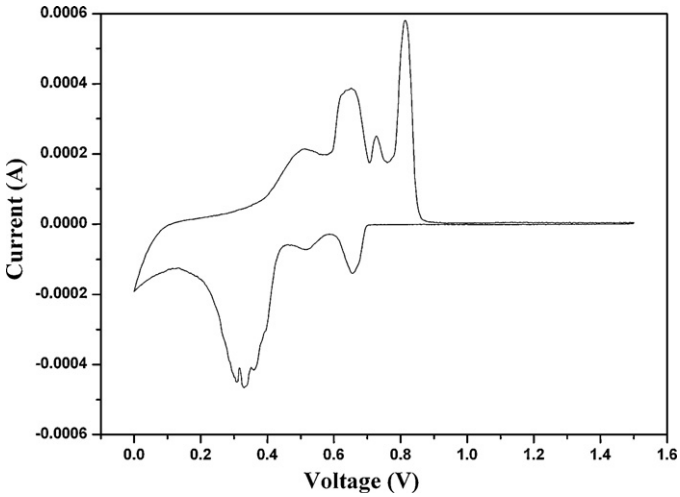

Fig. 7. Cyclic voltammogram curve of the Sn–Cu thin film electrode 5m9s cycled between 0 V and 1.5 V vs. Li/Li^+ with a scan rate of 0.05 mV s^{-1}.

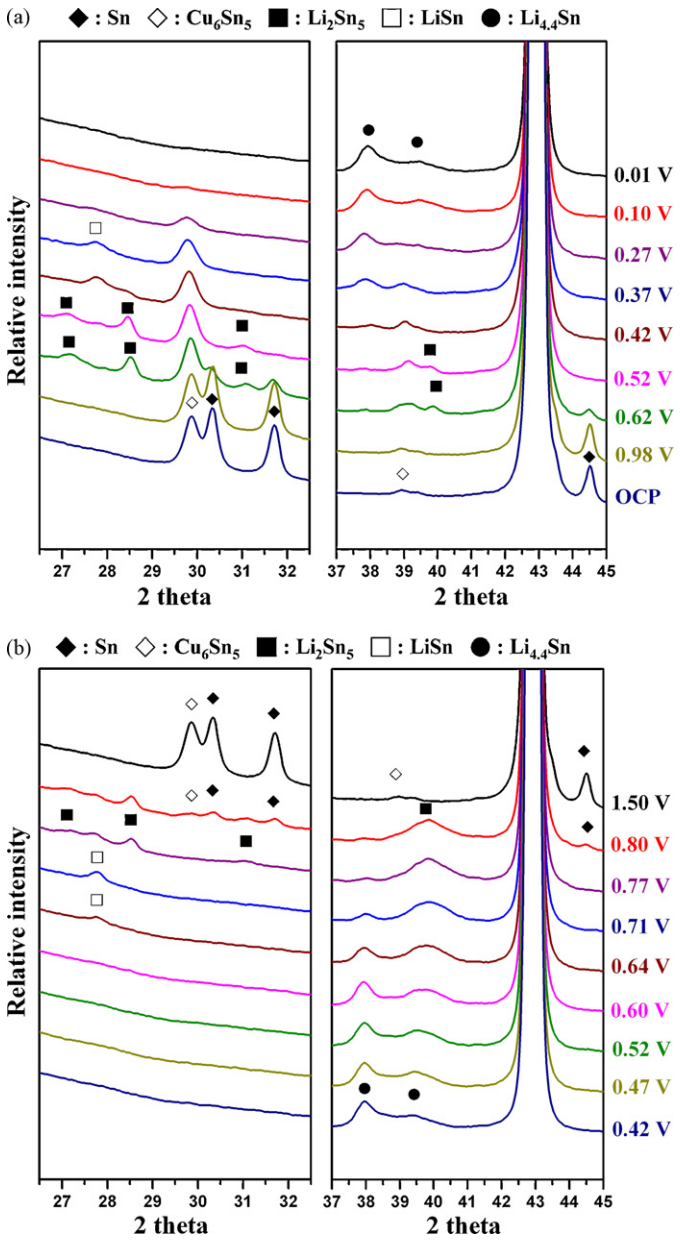

Fig. 8. In situ XRD analysis of the Sn–Cu thin film electrode 5m9s cycled between 0 V and 1.5 V vs. Li/Li^+ for the 15th cycle: (a) discharge process and (b) charge process.

phase. Once the cell reached 0.001 V, the pattern showed mainly the $Li_{4.4}Sn$ phase. In the process of lithium insertion, the phase of Li_2CuSn did not appear in the sequence of XRD patterns. Moreover, Fig. 8b exhibits in situ XRD patterns of cell during the subsequent charge process at 15th cycle. The in situ XRD patterns also showed continuous phase transformations of copper–tin alloy. When the voltage was increased to 0.64 V, $Li_{4.4}Sn$ alloy disappeared, and the phase of LiSn showed up. As the lithium was further extracted from LiSn alloy, Li_2Sn_5 reformed with the disappearance of LiSn phase at 0.77 V. As the voltage was above 0.80 V, pure Sn and Cu_6Sn_5 began to be generated. The phases were Cu_6Sn_5 and pure metallic Sn at the fully charged state. These phases were identical with those at the OCV state. It should be noted that the reactions between active material and lithium were reversible. In literature, different structures of Cu_6Sn_5 delivered different reaction paths during cycling [15,16]. When the Cu_6Sn_5 was high-temperature hexagonal phase, the phase transformations of Cu_6Sn_5 was via the formation of Li_2CuSn intermediate phase during cycling. The voltage plateaus and peaks were at 0.1 V and 0.4 V. However, as the Cu_6Sn_5 was low-temperature monoclinic phase, Cu_6Sn_5 reacted with lithium directly without the presence of Li_2CuSn phase. Nevertheless, the phase Li_2CuSn, which was the feature of high-temperature η-Cu_6Sn_5, was not shown during cycling. As a result, the reaction mechanism of copper–tin alloy was an alloying process [16], and the Cu_6Sn_5 alloy might be considered as the low-temperature η′-Cu_6Sn_5.

4. Conclusions

Sn–Cu thin film electrodes were synthesized by sputtering. Island Sn particles were deposited on the Cu foil and Cu_6Sn_5 was formed at the interface between Sn and Cu. Introducing Cu source into Sn-based anode by sputtering Sn/Cu alternately could enhance the cycling stability as compared with cell deposited only by Sn. Adjusting different sputtering time of Sn and Cu on the Cu foil alternately could change the phase and composition of electrode. As the deposition time of Sn and Cu was 5 min and 9 s, respectively, the cycling stability was the best. The initial capacity of cell was around 635 mA hg^{-1}, and 1st efficiency was as high as 97%. The capacity remained higher than 500 mA hg^{-1} after 15 cycles. The electrochemical lithiation reactions of Cu_6Sn_5 were not observed through voltage profile and CV curve. From the in situ XRD analysis, the transformation of Cu_6Sn_5 during cycling was visible. The phase of Cu_6Sn_5 transformed into Li–Sn alloy directly during cycling without the presence of Li_2CuSn. Therefore, the reaction mechanism of Cu_6Sn_5 was alloying process, and the Cu_6Sn_5 alloy might be considered as the low-temperature η′-Cu_6Sn_5.

Acknowledgements

The authors are grateful to National Science Council, Taiwan (No. NSC 96-2221-E-007-093) for the partial financial support. We also thank the group of Dr. Hwo-Shuenn Sheu for their technical assistance and the National Synchrotron Radiation Research Center (NRSSC) for the use of synchrotron X-ray diffraction facilities.

References

[1] H. Zheng, K. Jiang, T. Abe, Z. Ogumi, Carbon 44 (2006) 203–210.
[2] M. Winter, J.O. Besenhard, Electrochim. Acta 45 (2006) 31–50.
[3] I.A. Courtney, J.R. Dahn, J. Electrochem. Soc. 144 (1999) 2045–2052.
[4] L.Y. Beaulieu, K.W. Eberman, R.L. Turner, L.J. Krause, J.R. Dahn, Electrochem. Solid-State Lett. 4 (2001) A137–A140.
[5] H. Li, Q. Wang, L. Shi, L. Chen, X. Huang, Chem. Mater. 14 (2002) 103–108.
[6] P. Limthongkul, H. Wang, E. Jud, Y. Chiang, J. Electrochem. Soc. 149 (2002) A1237–A1245.
[7] I.A. Courtney, W.R. McKinnon, J.R. Dahn, J. Electrochem. Soc. 146 (1999) 59–68.
[8] H. Li, L. Shi, W. Lu, X. Huang, L. Chen, J. Electrochem. Soc. 148 (2001) A915–A922.
[9] D.G. Kim, H. Kim, H.-J. Sohn, T. Kang, J. Power Sources 104 (2002) 221–225.
[10] T. Sarakonsri, T. Apirattanawan, S. Tungprasurt, T. Tunkasiri, J. Mater. Sci. 41 (2006) 4749–4754.
[11] F. Wang, M. Zhao, X. Song, J. Alloys Compd. 439 (2007) 249–253.
[12] S.D. Beattie, J.R. Dahn, J. Electrochem. Soc. 150 (2003) C457–C460.
[13] J.W. Park, S. Rajendran, H.S. Kwon, J. Power Sources 159 (2006) 1409–1415.
[14] R.Z. Hu, Y. Zhang, M. Zhu, Electrochim. Acta 53 (2008) 3377–3385.
[15] G.X. Wang, L. Sun, D.H. Bradhurst, S.X. Dou, H.K. Liu, J. Alloys Compd. 299 (2000) L12–L15.
[16] K.-F. Chiu, K.M. Lin, H.C. Lin, W.Y. Chen, D.T. Shieh, J. Electrochem. Soc. 154 (2007) A433–A437.
[17] S. Sharma, L. Fransson, E. Sjöstedt, L. Nordström, B. Johansson, K. Edström, J. Electrochem. Soc. 150 (2003) A330–A334.
[18] D. Larcher, L.Y. Beaulieu, D.D. MacNeil, J.R. Dahn, J. Electrochem. Soc. 147 (2000) 1658–1662.